

# Phase-field modeling of crack propagation in multiphase systems

Daniel Schneider<sup>a,b,\*</sup>, Ephraim Schoof<sup>b</sup>, Yunfei Huang<sup>b</sup>, Michael Selzer<sup>a,b</sup>,  
Britta Nestler<sup>a,b</sup>

<sup>a</sup> Institute of Applied Materials (IAM-CMS), Karlsruhe Institute of Technology (KIT), Kaiserstrasse 12, 76131 Karlsruhe, Germany

<sup>b</sup> Institute of Materials and Processes (IMP), Karlsruhe University of Applied Sciences, Moltkestrasse 30, D-76133 Karlsruhe, Germany

Available online 19 April 2016

## Abstract

Modeling of crack propagation in materials has long been a challenge in solid-state physics and materials science. The phase-field method has now established as one of the tools for the description of crack propagation. The applied models are thermodynamically consistent and predict crack propagation in homogeneous materials under the consideration of different loading types, multiple physical fields and geometrical nonlinearities. Even dynamic loading processes are studied, including plastic effects. A multiphase-field model for crack propagation, which is indispensable to describe crack propagation on a mesoscopic length scale, is still missing. In this work, we overcome this deficiency and combine a crack propagation approach, which is based on Griffith's theory, with an established multiphase-field model for phase transformation.

© 2016 Elsevier B.V. All rights reserved.

*Keywords:* Phase-field; Multiphase-field; Polycrystalline material; Crack propagation

## 1. Introduction

Modeling of crack propagation in materials has long been a challenge in solid-state physics and materials science [1,2]. The uniform movement of cracks has been well understood in the context of theoretical continuum mechanics [3]. The energetic balance at the crack front is thereby described by the Griffith criterion [4]. A crack does propagate when the energy release rate at the crack front exceeds the surface energy, which is gained during crack growth. The conventional method for modeling crack propagation is the strict separation of the material into a destroyed region and an intact region, by means of a sharp interface. The local interface velocity can be described at the interface with the help of a balance equation. Still, such a procedure does require tracking of the exact position of the interface, which is computationally quite unfeasible when modeling complex three-dimensional systems [5]. Compared to sharp interface models, the phase-field method has a decisive advantage as explicit interface tracking becomes redundant [5].

\* Corresponding author at: Institute of Applied Materials (IAM-CMS), Karlsruhe Institute of Technology (KIT), Kaiserstrasse 12, 76131 Karlsruhe, Germany.

*E-mail addresses:* [daniel.schneider@kit.edu](mailto:daniel.schneider@kit.edu) (D. Schneider), [ephraim.schoof@hs-karlsruhe.de](mailto:ephraim.schoof@hs-karlsruhe.de) (E. Schoof), [yunfei.huang@hs-karlsruhe.de](mailto:yunfei.huang@hs-karlsruhe.de) (Y. Huang), [michael.selzer@kit.edu](mailto:michael.selzer@kit.edu) (M. Selzer), [britta.nestler@kit.edu](mailto:britta.nestler@kit.edu) (B. Nestler).

In the literature there are two types of phase-field models known to describe crack propagation: physical models, which are based on phase transitions of Ginzburg–Landau-type, and mechanical approaches based on Griffith's theory. Ambati et al. [6] provide a detailed overview of the existing models. All models use order parameters to separate between damaged and undamaged material. By minimization of the total system energy, the models describe the propagation of cracks [7]. The models are thermodynamically consistent and predict crack propagation in homogeneous materials under different loading types [8–10], including the effects of plasticity [11,12,6,13] and multi-physics problems [14–16]. Only few approaches describe crack propagation in heterogeneous materials. One of the first physical models is proposed by Spatschek et al. [17]. Extensions of this approach to plastic effects in multiphase materials are elaborated by Schneider et al. [18] and applications in ferroelectric polycrystals are shown by Abdollahi and Arias [19]. A similar physical approach is formulated by Oshima et al. [20]. To investigate the effective toughness of heterogeneous materials, Hossain et al. [21] employ a mechanical approach with heterogeneous crack resistance. But a multiphase-field model for crack propagation based on Griffith's theory is still missing.

In this work, we combine a mechanical approach for the description of crack propagation with the multiphase-field model of Nestler et al. [22]. We use a single-obstacle potential as an energetic potential and couple it with a multi-obstacle potential, which has established itself during the modeling of phase transition processes. We apply the model to predict crack propagation in binary systems as well as in polycrystalline materials on a mesoscopic length scale.

## 2. Phase-field model for crack propagation with a single-obstacle potential

For the description of the crack propagation, we employ the mechanical approach of Kuhn et al. [9] as the basis of our model formulation. We introduce an order parameter for the crack region  $\phi_c$ , which describes a continuous transition between the intact and the destroyed material. This allows a connection with a multiphase-field model. Regardless of whether the solid phase is single-phase or multiphase, the following derivation applies for the order parameter of the solid phase:  $\phi_s = 1 - \phi_c$ . The total energy of a system with a single solid phase is a function of the order parameter  $\phi_c$  and the displacement field  $\mathbf{u}$  and is given by

$$\mathcal{F}(\phi_c, \mathbf{u}) = \int G_c \left( \varepsilon |\nabla \phi_c|^2 + \frac{1}{\varepsilon} w_c(\phi_c) \right) + h_c(\phi_c) f_{el}(\mathbf{u}) dV, \quad (1)$$

where  $G_c$  is the crack resistance,  $h_c(\phi_c) = (1 - \phi_c)^2$  is the interpolation function,  $w_c(\phi_c)$  is the energy potential and  $f_{el}(\mathbf{u})$  is the strain energy density of the solid.  $\varepsilon$  represents a parameter for the width of the transition region. The elastic strain energy density is expressed as  $f_{el}(\mathbf{u}) = \boldsymbol{\epsilon}(\mathbf{u}) : \mathbf{C}^s[\boldsymbol{\epsilon}]/2 = \epsilon_{ij} (\mathbf{C}^s[\boldsymbol{\epsilon}])_{ij} / 2$  and depends on the symmetric local elastic strain  $\boldsymbol{\epsilon}(\mathbf{u})$ , which in turn depends on the displacement field  $\mathbf{u}$  by  $\boldsymbol{\epsilon}(\mathbf{u}) = (\nabla \mathbf{u} + (\nabla \mathbf{u})^T)/2$ . The gradient of the displacement field can be written as  $(\nabla \mathbf{u})_{ij} = \partial u_i / \partial x_j$ . The local stress state  $\boldsymbol{\sigma}$  relates to the elastic energy contribution by  $\partial f_{el}(\mathbf{u}) / \partial \epsilon_{ij} = (\mathbf{C}^s[\boldsymbol{\epsilon}])_{ij} = C_{ijkl}^s \epsilon_{kl} = (\boldsymbol{\sigma})_{ij}$ , where  $\mathbf{C}^s$  defines the stiffness tensor of the solid phase. The evolution of the order parameter is described by the Allen–Cahn equation [23]

$$\dot{\phi}_c = -M \frac{\delta \mathcal{F}(\phi_c, \mathbf{u})}{\delta \phi_c} = -M \left( \frac{\partial \mathcal{F}(\phi_c, \mathbf{u})}{\partial \phi_c} - \nabla \cdot \frac{\partial \mathcal{F}(\phi_c, \mathbf{u})}{\partial \nabla \phi_c} \right). \quad (2)$$

Only physically relevant changes,  $\dot{\phi}_c \geq 0$ , are accepted in order to prevent crack healing. We apply a simplified form of the mechanical driving force since our applications are under Mode-I load. A further extension of the driving force formulation is comprehensively described in Ambati et al. [6].

In the mechanical models, which describe crack propagation, the one-well potential  $w_{wel}(\phi_c) = \phi_c^2/4$  is usually used as the energy potential  $w_c(\phi_c)$  [6]. The potential enables a defined resistance against crack growth and the surface energy is depicted in such a way, that the Griffith criterion is fulfilled by the interface [9,6]. But the derivative of the potential vanishes at position  $\phi_c = 0$ , as in all double-well-type potentials. These potentials, therefore, lead to a widely extended profile of the order parameter, as shown in Fig. 1. Such a wide transition region is very unfavorable from a numerical point of view. An alternative is an obstacle-type potential, that is usually used to describe phase transition processes [22]. The obstacle-type potential fulfills the necessary properties for the description of phase transition processes and simultaneously offers a well-defined width of the transition region  $l$ . Therefore, the partial differential equations for the order parameters only need to be solved in a finite region of a diffuse interface layer [22]. Furthermore, the single-obstacle potential  $w_{ob1}(\phi_c)$  can be combined with a multi-obstacle potential  $w_{ob}(\phi_s)$  of the

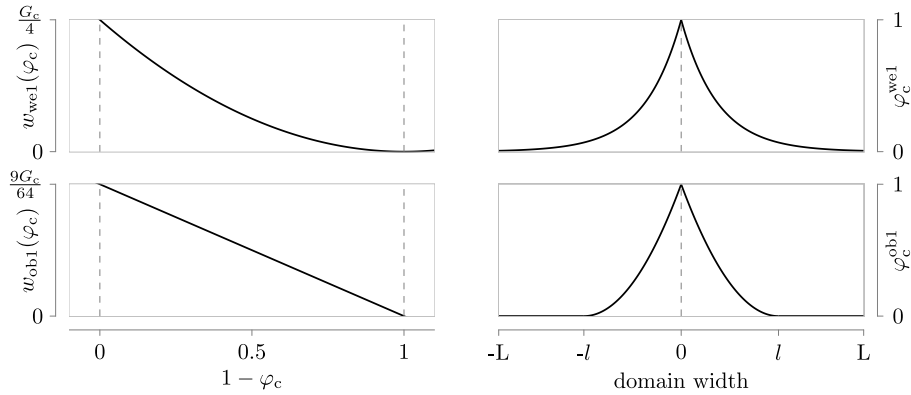


Fig. 1. Comparison of the equilibrium profiles using  $w_{we1}$  and  $w_{ob1}$  in a one-dimensional domain with a length of  $2L = 20\varepsilon$ . On the left, the potentials are shown and on the right, the resulting equilibrium profiles are displayed.

solid region consisting of e.g. multiple grains. The single-obstacle potential reads

$$w_c(\phi_c) = w_{ob1}(\phi_c) = K\phi_c, \quad (3)$$

with a constant  $K$ , which needs to be determined. We set  $w_c(\phi_c) = \infty$  if  $\phi_c$  is not in the range of  $0 \leq \phi_c \leq 1$ . Similar types of the potential are suggested by Bourdin et al. [24] and Hossain et al. [21].

For the determination of  $K$ , a one-dimensional system of  $2L$  in length, with a transition region at  $x = 0$ , is considered, as shown in Fig. 1. The profile of the order parameters is characterized by the equilibrium state  $\dot{\phi}_c = 0$ . With this, the gradients of  $\phi_c$ , in unloaded condition, result from the equipartition of the energy condition as

$$2\varepsilon \frac{\partial^2 \phi_c}{\partial x^2} = \frac{1}{\varepsilon} \frac{\partial w_c(\phi_c)}{\partial \phi_c} \quad (4)$$

$$\int_0^x 2 \frac{\partial \phi_c}{\partial x} \left( \frac{\partial^2 \phi_c}{\partial x^2} \right) dx = \frac{1}{\varepsilon^2} \int_0^x \frac{\partial \phi_c}{\partial x} \frac{\partial w_c(\phi_c)}{\partial \phi_c} dx \quad (5)$$

$$\left( \frac{\partial \phi_c}{\partial x} \right)^2 = \frac{1}{\varepsilon^2} w_c(\phi_c) \quad (6)$$

$$\frac{\partial \phi_c}{\partial x} = \pm \sqrt{\frac{1}{\varepsilon^2} w_c(\phi_c)}. \quad (7)$$

In order to fulfill the Griffith criterion [4] for the crack growth, the resulting interfacial energy  $\Gamma$  from an interface must be  $G_c/2$  [25]. This condition is fulfilled by the one-well potential  $w_{we1}(\phi_c)$ :

$$\Gamma = \int_0^L G_c \left( \varepsilon \left( \frac{\partial \phi_c}{\partial x} \right)^2 + \frac{1}{\varepsilon} w_{we1}(\phi_c) \right) dx \quad (8)$$

$$= \int_0^1 \frac{2G_c}{\varepsilon} w_{we1}(\phi_c) \frac{\partial x}{\partial \phi_c} d\phi_c = \int_0^1 2G_c \sqrt{w_{we1}(\phi_c)} d\phi_c \quad (9)$$

$$= G_c \int_0^1 \phi_c d\phi_c = \frac{G_c}{2}. \quad (10)$$

Now this condition is used to determine the factor  $K$  for the single-obstacle potential  $w_{ob1}$ :

$$\frac{G_c}{2} = \int_0^L G_c \left( \varepsilon \left( \frac{\partial \phi_c}{\partial x} \right)^2 + \frac{1}{\varepsilon} w_{ob1}(\phi_c) \right) dx \quad (11)$$

$$= \int_0^1 2G_c \sqrt{w_{ob1}(\phi_c)} d\phi_c = \frac{4}{3} G_c \sqrt{K}. \quad (12)$$

Thus, the selection of  $K = 9/64$  for the single-obstacle potential  $w_{\text{ob1}}(\phi_c)$  fulfills the energetic Griffith criterion for the crack growth from the side of the interfacial energy. With the prefactor  $K$ , the width of the transition region gives

$$l = \int_0^1 \frac{\partial x}{\partial \phi_c} d\phi_c = \frac{16}{3}\varepsilon. \quad (13)$$

Accordingly, the profile of the order parameter results in

$$\phi_c(x) = \left(1 - \frac{3}{16\varepsilon}|x|\right)^2, \quad -l < x < l. \quad (14)$$

The profiles of the potentials  $w_{\text{we1}}(\phi_c)$  and  $w_{\text{ob1}}(\phi_c)$  and the interface regions are compared in Fig. 1. Using the single-obstacle potential  $w_{\text{ob1}}(\phi_c)$  leads to a well-defined profile with a width of  $2l$ .

### 3. Multiphase-field model for crack propagation

In the next step, the crack propagation model is combined with the multiphase-field model of Nestler et al. [22]. In a system of  $N$  phases, the order parameter  $\phi_c$  is still used for the crack region. In the solid region, the remaining  $N - 1$  order parameters are collected in a tuple  $\phi_s = \phi_1, \dots, \phi_{N-1}$ . This yields the following total energy functional:

$$\begin{aligned} \mathcal{F}(\phi, \mathbf{u}) = & \int G_c(\phi_s) \left( \varepsilon_c |\nabla \phi_c|^2 + \frac{1}{\varepsilon_c} w_c(\phi_c) \right) + h_c(\phi_c) f_{\text{el}}(\mathbf{u}, \phi_s) \\ & + \varepsilon_s a(\phi_s, \nabla \phi_s) + \frac{1}{\varepsilon_s} w_{\text{ob}}(\phi_s) dV, \end{aligned} \quad (15)$$

where  $a(\phi_s, \nabla \phi_s)$  defines a general gradient energy density for multiphase/multi-grain systems of the form

$$a(\phi_s, \nabla \phi_s) = \sum_{\alpha \neq c} \sum_{\beta > \alpha \neq c} \gamma_{\alpha\beta} |\phi_\alpha \nabla \phi_\beta - \phi_\beta \nabla \phi_\alpha|^2 \quad (16)$$

and the energy potential in the solid region can be written as,

$$w_{\text{ob}}(\phi_s) = \frac{16}{\pi^2} \sum_{\alpha \neq c} \sum_{\beta > \alpha \neq c} \gamma_{\alpha\beta} \phi_\alpha \phi_\beta + \sum_{\alpha, \beta > \alpha, \delta > \beta} \gamma_{\alpha\beta\delta} \phi_\alpha \phi_\beta \phi_\delta. \quad (17)$$

The additional three-phase contribution in the potential prevents the non-physical development of the so-called third phases [22] in the two-phase region. The effect of the higher order term is illustrated in Fig. 2. This contribution increases the potential in the triple point region, so that the conversion in this region becomes energetically unfavorable. A comprehensive discussion of this term can be found in Hoetzer et al. [26]. Similar to the two-phase case, we set  $w_c(\phi_c) + w_{\text{ob}}(\phi_s) = \infty$  if the  $n$ -tuple of the order parameters  $\phi = \phi_1, \dots, \phi_N$  is not on the Gibbs simplex

$$\mathcal{G} = \left\{ \phi \in \mathbb{R}^N : \sum_{\alpha} \phi_{\alpha} = 1, \phi_{\alpha} \geq 0 \right\}, \quad (18)$$

as described by Nestler et al. [22]. As the width of the transition regions is different in the solid region and the crack region, two parameters,  $\varepsilon_c$  and  $\varepsilon_s$ , respectively, are introduced for the interface width. The crack resistance  $G_c(\phi_s)$  and the strain energy density  $f_{\text{el}}(\mathbf{u}, \phi_s)$  are dependent on the local microstructure. For the interpolation of these terms, the usual antisymmetric interpolation functions can be used (see, for example, [22]). However, it should be ensured that the condition  $\sum_{\alpha} h^{\alpha}(\phi) = 1$  is always fulfilled [27]. Therefore, we use the following phase-dependent and standardized interpolation function for the solid region:

$$h_s^{\alpha}(\phi_s) = \frac{\phi_{\alpha}^2(3 - 2\phi_{\alpha})}{\sum_{\beta \neq c} \phi_{\beta}^2(3 - 2\phi_{\beta})}. \quad (19)$$

For the crack phase, the interpolation function  $h_c = (1 - \phi_c)^2$  still holds and has not to be normalized explicitly, since it is applied in a quasi-two-phase case. This results in the energetic crack resistance

$$G_c(\phi_s) = \sum_{\alpha \neq c} G_c^{\alpha} h_s^{\alpha}(\phi_s) \quad (20)$$

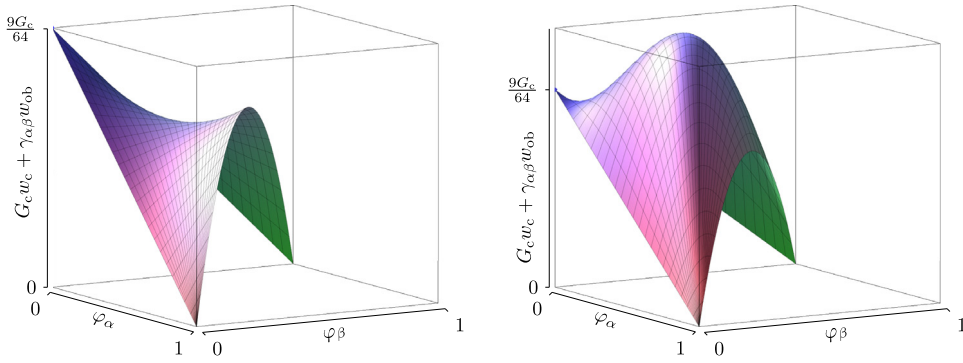


Fig. 2. Comparison of the resulting combined potentials on a triple junction with a crack phase without (left) and with (right) the third phase term.

and for the strain energy density, we correspondingly obtain

$$f_{\text{el}}(\mathbf{u}, \boldsymbol{\phi}_s) = \sum_{\alpha \neq c} f_{\text{el}}^\alpha(\mathbf{u}) h_s^\alpha(\boldsymbol{\phi}_s), \quad (21)$$

with  $G_c^\alpha$  as the energetic crack resistance and  $f_{\text{el}}^\alpha(\mathbf{u}) = \boldsymbol{\epsilon}(\mathbf{u}) : \mathbf{C}^\alpha[\boldsymbol{\epsilon}(\mathbf{u})]/2$  as the strain energy density of the respective phase  $\alpha$ . We use this form of the strain energy density for the mechanical driving force and for phase transitions, respectively, since our applications are under Mode-I load. A further extension of the driving force formulation is comprehensively described in Ambati et al. [6].

The variational approach in the presence of the additional constraint  $\sum_\alpha \phi_\alpha = 1$  leads to the following conditions for each phase:

$$0 = \frac{\delta \mathcal{F}}{\delta \phi_\alpha} - \frac{1}{N} \sum_\beta \frac{\delta \mathcal{F}}{\delta \phi_\beta}, \quad \forall \phi_\alpha, \alpha = 1, \dots, N, \quad (22)$$

as described in [22]. Since the mobilities of the interfaces in this combined system vary considerably, the condition (22) is initially split into dual contributions, and an individual mobility,  $M_{\alpha\beta}$ , is subsequently introduced for each  $\alpha$ – $\beta$  interface. This leads to Allen–Cahn equations for each single phase in the multiphase system, with different mobilities of the interfaces:

$$\dot{\phi}_\alpha = -\frac{1}{N} \sum_{\beta \neq \alpha} M_{\alpha\beta} \left( \frac{\delta \mathcal{F}}{\delta \phi_\alpha} - \frac{\delta \mathcal{F}}{\delta \phi_\beta} \right), \quad \forall \phi_\alpha, \alpha = 1, \dots, N. \quad (23)$$

Such an approach was already used by Steinbach and Pezzolla in [28]. If the variational derivative is performed for the crack phase  $\phi_c$ , this results in

$$\frac{\delta \mathcal{F}}{\delta \phi_c} = \frac{G_c(\boldsymbol{\phi}_s)}{\varepsilon} K - 2\varepsilon_c \nabla \cdot (G_c(\boldsymbol{\phi}_s) \nabla \phi_c) + \frac{\partial h_c(\phi_c)}{\partial \phi_c} f_{\text{el}}(\mathbf{u}, \boldsymbol{\phi}_s). \quad (24)$$

If the variation is calculated with respect to one of the solid phases  $\alpha \neq c$ , we derive

$$\begin{aligned} \frac{\delta \mathcal{F}}{\delta \phi_\alpha} = & \frac{\partial G_c(\boldsymbol{\phi}_s)}{\partial \phi_\alpha} \left( \varepsilon_c |\nabla \phi_c|^2 + \frac{1}{\varepsilon_c} w_c(\phi_c) \right) + h_c(\phi_c) \frac{\partial f_{\text{el}}(\mathbf{u}, \boldsymbol{\phi}_s)}{\partial \phi_\alpha} \\ & + \frac{\partial a(\boldsymbol{\phi}_s, \nabla \boldsymbol{\phi}_s)}{\partial \phi_\alpha} - \nabla \cdot \frac{\partial a(\boldsymbol{\phi}_s, \nabla \boldsymbol{\phi}_s)}{\partial \nabla \phi_\alpha} + \frac{\partial \omega_{\text{ob}}(\boldsymbol{\phi}_s)}{\partial \phi_\alpha}. \end{aligned} \quad (25)$$

Reducing the system to two phases, i.e. one crack phase  $\phi_c$  and one solid phase  $\phi_s$ , the evolution equation (23) simplifies to Eq. (2) with  $M_{sc} = 2M$ . In the variation of the functional (15) with respect to the crack phase  $\phi_c$ , the grain boundary energy of the solid phases  $\gamma_{\alpha\beta}$  is not listed explicitly. But the evolution equation for the order parameters (23) couples the dual interactions between all phases. Therefore, the grain boundary energy  $\gamma_{\alpha\beta}$  is taken into account for the evolution of the crack phase, even if the mobility of the solid phases vanishes.

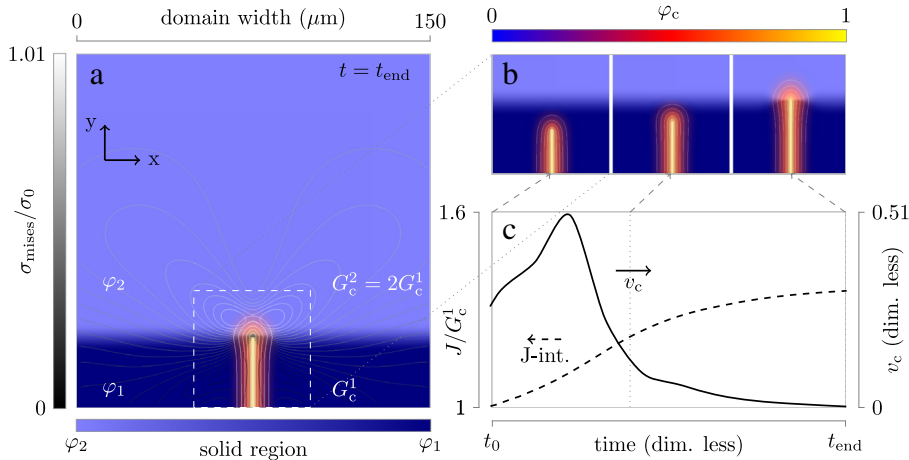


Fig. 3. Influence of a horizontal grain boundary: (a) Simulation setup with two solid phases and the profile of  $\sigma_{\text{mises}}$  at  $t = t_{\text{end}}$ , (b) evolution of the crack phase  $\phi_c$  and (c)  $J$ -Integral  $J$  and the crack tip velocity  $v_c$ .

#### 4. Numerical implementation

The simulations in this work are performed with the Pace3D software package, version 2.1.1. In order to describe the geometry, various order parameters are used for the different physical regions. The evolution of the order parameters (Eqs. (2) and (23)) is solved on an equidistant grid with an explicit Euler method. At the same time, the mechanical equilibrium condition  $\nabla \cdot \boldsymbol{\sigma} = \mathbf{0}$  is implicitly calculated in every time step.

#### 5. Numerical examples

The following simulation study demonstrates the applicability of the presented model for the description of crack propagation in multiphase/multi-grain systems. The verification of the used potential in a homogeneous material has already been discussed in detail in Bourdin et al. [24] and Hossain et al. [21]. Therefore, we directly demonstrate simulation studies of applications in heterogeneous materials.

First, we investigate the influence of a horizontal grain boundary on the crack tip velocity. A simulation domain with two solid phases,  $\phi_1$  and  $\phi_2$ , is set in a two-dimensional domain, forming a horizontal grain boundary, as pictured in Fig. 3(a). Both solid phases have the same isotropic material parameters of steel, with a Young's modulus of  $E_0 = 210$  GPa and a Poisson's ratio of  $\nu = 0.3$ . Therefore, there is no influence on the stresses through the grain boundary, as demonstrated by the profile of the von Mises stress  $\sigma_{\text{mises}}$  in Fig. 3(a). The grain boundary energy is  $\gamma_{12} = 0.1G_c^1$  and the crack resistances are taken as  $G_c^2 = 2G_c^1$ . We use a plane strain condition and the imposed load is applied by a displacement boundary condition in  $x$ -direction, while the boundary in  $y$ -direction stays strain-free. For the order parameter fields, a Neumann boundary condition is used. To prevent a phase transition between the solid phases, we set the mobility of the solid–solid grain boundary  $M_{12}$  to zero but ensure a fully established interface in the initial state.

Since the energy release rate, calculated by the  $J$ -integral, exceeds the crack resistance  $G_c^1$ , the crack propagates. Reaching the grain boundary region, the crack tip velocity rises because the interfacial energy  $\gamma_{12}$  degrades additionally, as shown in Fig. 3(c). This influence of the interfacial energy will be investigated more accurately in the following numerical example. The crack resistance increases at this position and the crack velocity drops to a standstill.

One of the main advantages of the presented model is the possibility to set the mobility of several interfaces to zero but to consider the interfacial energy of those interfaces. This influence of the interfacial energy on the crack path is examined in this numerical example. We set an oblique grain boundary along the way of the crack, as shown in Fig. 4(a), choose equal mechanical properties as well as the crack resistances  $G_c^1 = G_c^2 = G_c$  for both solid phases  $\phi_1$  and  $\phi_2$  and vary the interfacial energy  $\gamma_{12}$ . The chosen boundary conditions are the same as in the last numerical example. In the initial step, we ensure a fully developed interface between the solid phases and set the solid–solid mobility to zero.

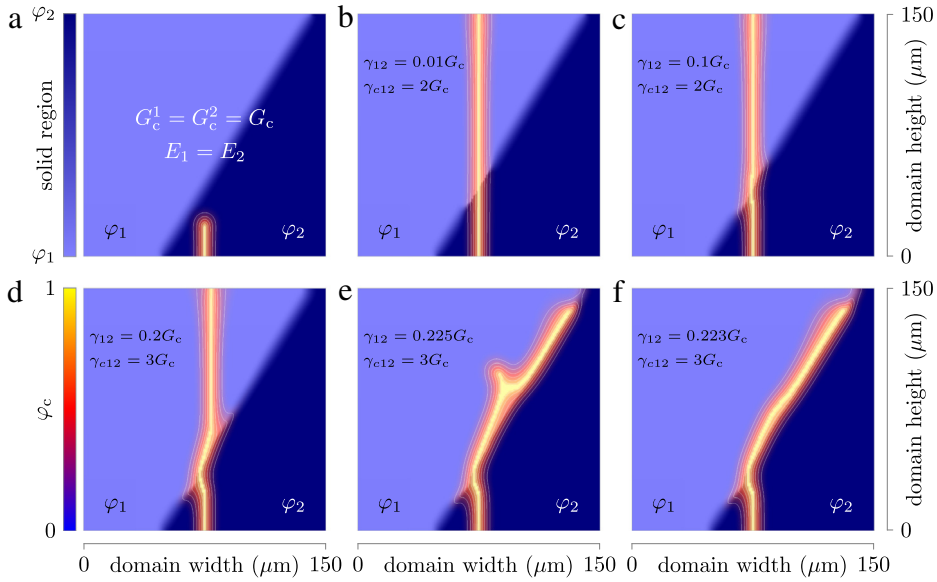


Fig. 4. Influence of an oblique grain boundary. The simulation setup with two solid phases and the crack phase with the corresponding isolines at the initial time step are shown in (a). The images (b)–(f) visualize the resulting crack path for different interfacial energies  $\gamma_{12}$ .

Small interfacial energies  $\gamma_{12} = 0.01G_c$  do not influence the crack path, as well as the profile of the order parameter  $\phi_c$ , as shown in the plotted isolines in Fig. 4(b). With increasing interfacial energy, the profile of  $\phi_c$  and the crack path are affected. In the underlying simulation setup, the critical value of  $\gamma_{12}$  is  $0.225G_c$ . Such a strong interfacial energy leads to a total deflection of the crack, as can be seen in Fig. 4(e). Even a splitting of the crack is appreciated in this simulation. For larger values of  $\gamma_{12}$ , only intercrystalline crack paths are evident.

In the last numerical example, we demonstrate crack propagation of a multiphase system. A simulation domain with five solid phases, each with a different Young's modulus  $E_\alpha$  and a different crack resistance  $G_c^\alpha$ , is prepared, as pictured in Fig. 5(a). The boundary conditions are the same as in the first numerical example. We ensure a fully developed interface between the solid phases in the initial state and set the solid–solid mobilities to zero. The crack path varies depending on the local elastic energy density  $f_{el}(\mathbf{u}, \phi_s)$ , the local crack resistance  $G_c(\phi_s)$  and the local grain boundary energy  $\gamma_{\alpha\beta}$ , as shown in Fig. 5(b)–(d). Both a transcrystalline as well as an intercrystalline crack propagation are clearly evident.

## 6. Conclusion and outlook

In this work, we presented a multiphase-field model to describe crack propagation in multiphase/multi-grain systems. For this purpose, we successfully coupled two different energy potentials in a multiphase-field model. This procedure allows the description of crack propagation processes in a solid region with heterogeneous and phase-dependent material parameters. Regardless of the chosen mobility of solid–solid interfaces, we demonstrate that the grain boundary energies influence the crack path. With this, we have taken a step forward to describe crack propagation in multiphase systems on a mesoscopic length scale. Additionally, the diffuse interface region between the solid phases makes it possible to modify the crack resistance at the grain boundaries. Ankit et al. [29] employ a similar approach to modify the diffusivities. Since the obstacle-type potential has a defined transition region, it is possible to reduce the local existing phases in a multiphase system [30,31]. Such a procedure makes a large-scale simulation in multi-grain systems with the phase-field method at all possible, as shown in [32–37].

The proposed model offers the possibility to investigate a crack propagation and a phase transformation process of solid phases simultaneously. One example is the martensitic transformation coupled with crack propagation, as discussed in [38]. An interesting topic is the investigation of such a coupled process in a multiphase/multi-grain system. With additional extension to tension–compression sensitivity, applications in cast iron are possible, as discussed in [39]. Nevertheless, we used the general linear interpolation methods for the calculation of the stresses and the driving forces in the solid region. In our preliminary work [40], we have already described the effects of the

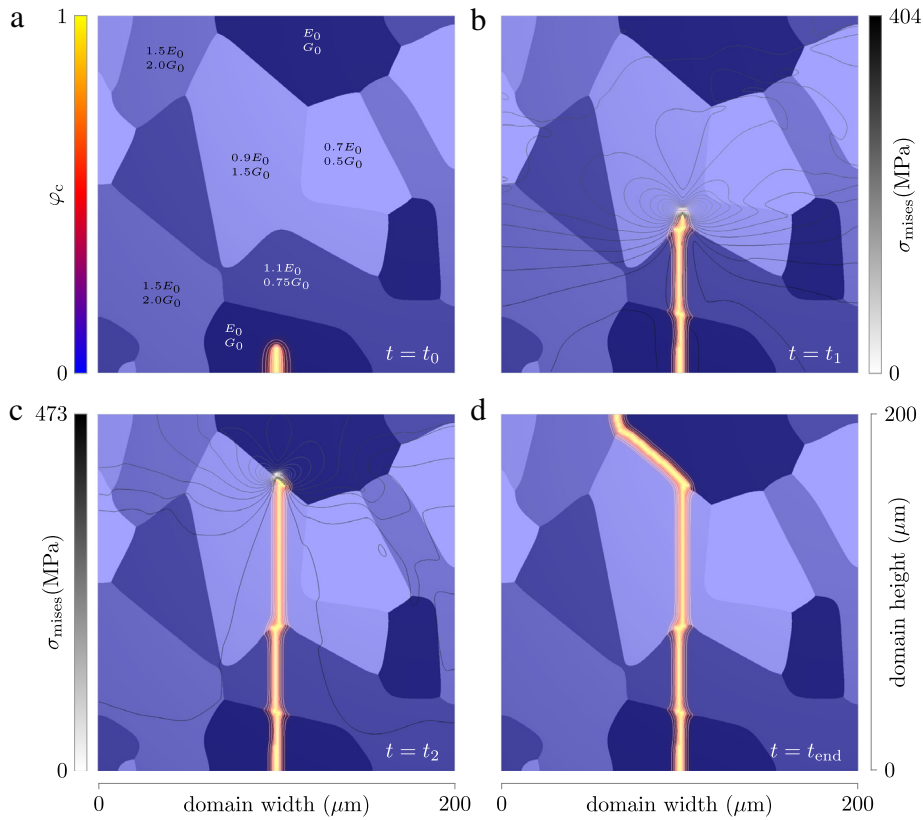


Fig. 5. Crack propagation in multiphase material. Figure (a) visualizes the microstructure of the initial state with the chosen material parameters. The highlighted phase-dependent material parameters are multiples of  $E_0 = 210$  GPa and  $G_0 = 1$  J/m<sup>2</sup> correspondingly. The snapshots (b)–(d) show the corresponding evolution of the black-colored crack phase and the profile of  $\sigma_{mises}$ . We remark that the grain boundaries are displayed as sharp contour lines, although the transition region between the solid phases is diffused as a result of the phase-field approach.

interpolation functions and derived a formulation that is capable of fulfilling the mechanical jump conditions. In our forthcoming work, we intend to couple the present multiphase-field model for crack propagation with the achieved novel interpolation scheme. Furthermore, the model should be extended by a phase-dependent plasticity formulation and a large deformation description.

## Acknowledgments

We thank the DFG for funding our investigations in the framework of the Research Training Group 1483 and the International Research Training Group 2078. The work was further supported by the state of Baden-Wuerttemberg and the European Regional Development Fund with a center of excellence in Computational Materials Science and Engineering and by the Helmholtz Portfolio topic “Materials Science for Energy and its Applications in Thin Film Photovoltaics and in Energy Efficiency”.

## References

- [1] M. Marder, J. Fineberg, How things break, *Phys. Today* 49 (9) (1996) 24. <http://dx.doi.org/10.1063/1.881515>.
- [2] B. Lawn, *Fracture of Brittle Solids*, Cambridge University Press, New York, 1993.
- [3] L.B. Freund, *Dynamic Fracture Mechanics*, Cambridge University Press, New York, 1998.
- [4] A.A. Griffith, The phenomena of rupture and flow in solids, *Phil. Trans. R. Soc. A* 221 (582–593) (1921) 163–198. <http://dx.doi.org/10.1098/rsta.1921.0006>.
- [5] L.-Q. Chen, Phase-field models for microstructure evolution, *Annu. Rev. Mater. Res.* 32 (1) (2002) 113–140. <http://dx.doi.org/10.1146/annurev.matsci.32.112001.132041>.

- [6] M. Ambati, T. Gerasimov, L. De Lorenzis, Phase-field modeling of ductile fracture, *Comput. Mech.* 55 (5) (2015) 1017–1040. <http://dx.doi.org/10.1007/s00466-015-1151-4>.
- [7] A. Karma, D. Kessler, H. Levine, Phase-Field model of mode III dynamic fracture, *Phys. Rev. Lett.* 87 (4) (2001) 3–6. <http://dx.doi.org/10.1103/PhysRevLett.87.045501>.
- [8] B. Bourdin, G. a. Francfort, J.-J. Marigo, *The Variational Approach to Fracture*, Vol. 91, Springer, Netherlands, Dordrecht, 2008. <http://dx.doi.org/10.1007/978-1-4020-6395-4>.
- [9] C. Kuhn, R. Müller, A continuum phase field model for fracture, *Eng. Fract. Mech.* 77 (18) (2010) 3625–3634. <http://dx.doi.org/10.1016/j.engfracmech.2010.08.009>.
- [10] C. Miehe, F. Welschinger, M. Hofacker, Thermodynamically consistent phase-field models of fracture: Variational principles and multi-field FE implementations, *Internat. J. Numer. Methods Engrg.* 83 (10) (2010) 1273–1311. <http://dx.doi.org/10.1002/nme.2861>.
- [11] M. Hofacker, C. Miehe, A phase field model for ductile to brittle failure mode transition, *PAMM* 12 (1) (2012) 173–174. <http://dx.doi.org/10.1002/pamm.201210077>.
- [12] F.P. Duda, A. Ciaronetti, P.J. Sánchez, A.E. Huespe, A phase-field/gradient damage model for brittle fracture in elastic–plastic solids, *Int. J. Plast.* 65 (2015) 269–296. <http://dx.doi.org/10.1016/j.ijplas.2014.09.005>.
- [13] M. Ambati, L. De Lorenzis, Phase-field modeling of brittle and ductile fracture in shells with isogeometric NURBS-based solid-shell elements, *Comput. Methods Appl. Mech. Engrg.* <http://dx.doi.org/10.1016/j.cma.2016.02.017>.
- [14] C. Miehe, L.-M. Schänzel, H. Ulmer, Phase field modeling of fracture in multi-physics problems. Part I. Balance of crack surface and failure criteria for brittle crack propagation in thermo-elastic solids, *Comput. Methods Appl. Mech. Engrg.* 294 (2015) 449–485. <http://dx.doi.org/10.1016/j.cma.2014.11.016>.
- [15] C. Miehe, M. Hofacker, L.-M. Schänzel, F. Aldakheel, Phase field modeling of fracture in multi-physics problems. Part II. Coupled brittle-to-ductile failure criteria and crack propagation in thermo-elastic–plastic solids, *Comput. Methods Appl. Mech. Engrg.* 294 (2015) 486–522. <http://dx.doi.org/10.1016/j.cma.2014.11.017>.
- [16] D. Schneider, M. Selzer, J. Bette, I. Rementeria, A. Vondrous, M.J. Hoffmann, B. Nestler, Phase-Field modeling of diffusion coupled crack propagation processes, *Adv. Energy Mater.* 16 (2) (2014) 142–146. <http://dx.doi.org/10.1002/adem.201300073>.
- [17] R. Spatschek, C. Müller-Gugenberger, E. Brener, B. Nestler, Phase field modeling of fracture and stress-induced phase transitions, *Phys. Rev. E* 75 (6) (2007) 1–14. <http://dx.doi.org/10.1103/PhysRevE.75.066111>.
- [18] D. Schneider, S. Schmid, M. Selzer, T. Böhlke, B. Nestler, Small strain elasto-plastic multiphase-field model, *Comput. Mech.* 55 (1) (2015) 27–35. <http://dx.doi.org/10.1007/s00466-014-1080-7>.
- [19] A. Abdollahi, I. Arias, Numerical simulation of intergranular and transgranular crack propagation in ferroelectric polycrystals, *Int. J. Fract.* 174 (1) (2012) 3–15. <http://dx.doi.org/10.1007/s10704-011-9664-0>.
- [20] K. Oshima, T. Takaki, M. Muramatsu, Development of multi-phase-field crack model for crack propagation in polycrystal, *Internat. J. Comput. Mater. Sci. Eng.* 03 (02) (2014) 1450009. <http://dx.doi.org/10.1142/S2047684114500092>.
- [21] M. Hossain, C.-J. Hsueh, B. Bourdin, K. Bhattacharya, Effective toughness of heterogeneous media, *J. Mech. Phys. Solids* 71 (2014) 15–32. <http://dx.doi.org/10.1016/j.jmps.2014.06.002>.
- [22] B. Nestler, H. Garcke, B. Stinner, Multicomponent alloy solidification: Phase-field modeling and simulations, *Phys. Rev. E* 71 (4) (2005) 041609. <http://dx.doi.org/10.1103/PhysRevE.71.041609>.
- [23] J.W. Cahn, S.M. Allen, A microscopic theory for domain wall motion and its experimental verification in Fe-Al alloy domain growth kinetics, *J. Phys. Colloq.* 38 (C7) (1977) C7–51–C7–54. <http://dx.doi.org/10.1051/jphyscol:1977709>.
- [24] B. Bourdin, J.-J. Marigo, C. Maurini, P. Sicsic, Morphogenesis and propagation of complex cracks induced by thermal shocks, *Phys. Rev. Lett.* 112 (1) (2014) 014301. <http://dx.doi.org/10.1103/PhysRevLett.112.014301>. [arXiv:1310.0501](https://arxiv.org/abs/1310.0501).
- [25] B. Bourdin, G. Francfort, J.-J. Marigo, Numerical experiments in revisited brittle fracture, *J. Mech. Phys. Solids* 48 (4) (2000) 797–826. [http://dx.doi.org/10.1016/S0022-5096\(99\)00028-9](http://dx.doi.org/10.1016/S0022-5096(99)00028-9).
- [26] J. Hötzer, O. Tschukin, M.B. Said, M. Berghoff, M. Jainta, G. Barthelemy, N. Smorchkov, D. Schneider, M. Selzer, B. Nestler, Calibration of a multi-phase field model with quantitative angle measurement, *J. Mater. Sci.* 51 (4) (2016) 1788–1797. <http://dx.doi.org/10.1007/s10853-015-9542-7>.
- [27] N. Moelans, A quantitative and thermodynamically consistent phase-field interpolation function for multi-phase systems, *Acta Mater.* 59 (3) (2011) 1077–1086. <http://dx.doi.org/10.1016/j.actamat.2010.10.038>.
- [28] I. Steinbach, F. Pezzolla, A generalized field method for multiphase transformations using interface fields, *Physica D* 134 (4) (1999) 385–393. [http://dx.doi.org/10.1016/S0167-2789\(99\)00129-3](http://dx.doi.org/10.1016/S0167-2789(99)00129-3).
- [29] K. Ankit, R. Mukherjee, T. Mittnacht, B. Nestler, Deviations from cooperative growth mode during eutectoid transformation: Insights from a phase-field approach, *Acta Mater.* 81 (2014) 204–210. <http://dx.doi.org/10.1016/j.actamat.2014.08.015>. [arXiv:arXiv:1408.1571v1](https://arxiv.org/abs/1408.1571v1).
- [30] S.G. Kim, D.I. Kim, W.T. Kim, Y.B. Park, Computer simulations of two-dimensional and three-dimensional ideal grain growth, *Phys. Rev. E* (3) 74 (6 Pt 1) (2006) 061605. <http://dx.doi.org/10.1103/PhysRevE.74.061605>.
- [31] B. Nestler, M. Reichert, M. Selzer, Massive multi-phase-field simulations: methods to compute large grain system, in: *Proceedings of the 11th International Conference on Aluminium Alloys, 2008*, pp. 1251–1255.
- [32] A. Vondrous, P. Bienger, S. Schreijäg, M. Selzer, D. Schneider, B. Nestler, D. Helm, R. Mönig, Combined crystal plasticity and phase-field method for recrystallization in a process chain of sheet metal production, *Comput. Mech.* 55 (2) (2015) 439–452. <http://dx.doi.org/10.1007/s00466-014-1115-0>.
- [33] J. Hötzer, M. Jainta, P. Steinmetz, B. Nestler, A. Dennstedt, A. Genau, M. Bauer, H. Köstler, U. Rüdte, Large scale phase-field simulations of directional ternary eutectic solidification, *Acta Mater.* 93 (2015) 194–204. <http://dx.doi.org/10.1016/j.actamat.2015.03.051>.
- [34] J. Hötzer, P. Steinmetz, M. Jainta, S. Schulz, M. Kellner, B. Nestler, A. Genau, A. Dennstedt, M. Bauer, H. Köstler, U. Rüdte, Phase-field simulations of spiral growth during directional ternary eutectic solidification, *Acta Mater.* 106 (2016) 249–259. <http://dx.doi.org/10.1016/j.actamat.2015.12.052>.

- [35] P. Steinmetz, Y.C. Yabansu, J. Hötzer, M. Jainta, B. Nestler, S.R. Kalidindi, Analytics for microstructure datasets produced by phase-field simulations, *Acta Mater.* 103 (2016) 192–203. <http://dx.doi.org/10.1016/j.actamat.2015.09.047>.
- [36] P. Steinmetz, J. Hötzer, M. Kellner, A. Dennstedt, B. Nestler, Large-scale phase-field simulations of ternary eutectic microstructure evolution, *Comput. Mater. Sci.* 117 (2016) 205–214. <http://dx.doi.org/10.1016/j.commatsci.2016.02.001>.
- [37] M. Bauer, U. Råde, J. Hötzer, M. Jainta, P. Steinmetz, M. Berghoff, F. Schornbaum, C. Godenschwager, H. Köstler, B. Nestler, Massively parallel phase-field simulations for ternary eutectic directional solidification, in: *Proceedings of the International Conference for High Performance Computing, Networking, Storage and Analysis - SC'15*, ACM Press, New York, USA, 2015, pp. 1–12. <http://dx.doi.org/10.1145/2807591.2807662>.
- [38] R. Schmitt, C. Kuhn, R. Skorupski, M. Smaga, D. Eifler, R. Müller, A combined phase field approach for martensitic transformations and damage, *Arch. Appl. Mech.* 85 (9–10) (2015) 1459–1468. <http://dx.doi.org/10.1007/s00419-014-0945-8>.
- [39] S. Schmid, D. Schneider, C. Herrmann, M. Selzer, B. Nestler, A Multiscale approach for thermo-mechanical simulations of loading courses in cast iron brake discs, *Internat. J. Multiscale Comput. Eng.* <http://dx.doi.org/10.1615/IntJMultCompEng.2015014764>.
- [40] D. Schneider, O. Tschukin, A. Choudhury, M. Selzer, T. Böhlke, B. Nestler, Phase-field elasticity model based on mechanical jump conditions, *Comput. Mech.* 55 (5) (2015) 887–901. <http://dx.doi.org/10.1007/s00466-015-1141-6>.